Supporting information

Facile Synthesis of Nickel Phosphide @ N-Doped Carbon Nanorods with Exceptional Cycling Stability as Li-Ion and Na-Ion Battery Anode Material

Fang Fu [1,†], Qiuchen He [1,†], Xuan Zhang [2], Julian Key [1,*], Peikang Shen [1] and Jinliang Zhu [1,*]

[1] Collaborative Innovation Center of Sustainable Energy Materials, Guangxi Key Laboratory of
Electrochemical Energy Materials, Guangxi University, Nanning 530004, China;
2015301022@st.gxu.edu.cn (F.F.); heqiuchen0817@163.com (Q.H.); pkshen@gxu.edu.cn (P.S.)
[2] Gansu Yinguang Chemical Industry Ltd., Baiyin 730900, China; zhangxy666@foxmail.com
* Correspondence: joolskey@yahoo.com (J.K.); jlzhu@gxu.edu.cn (J.Z.)
† These authors contributed equally to this work.

1. Experimental data and literature comparisons

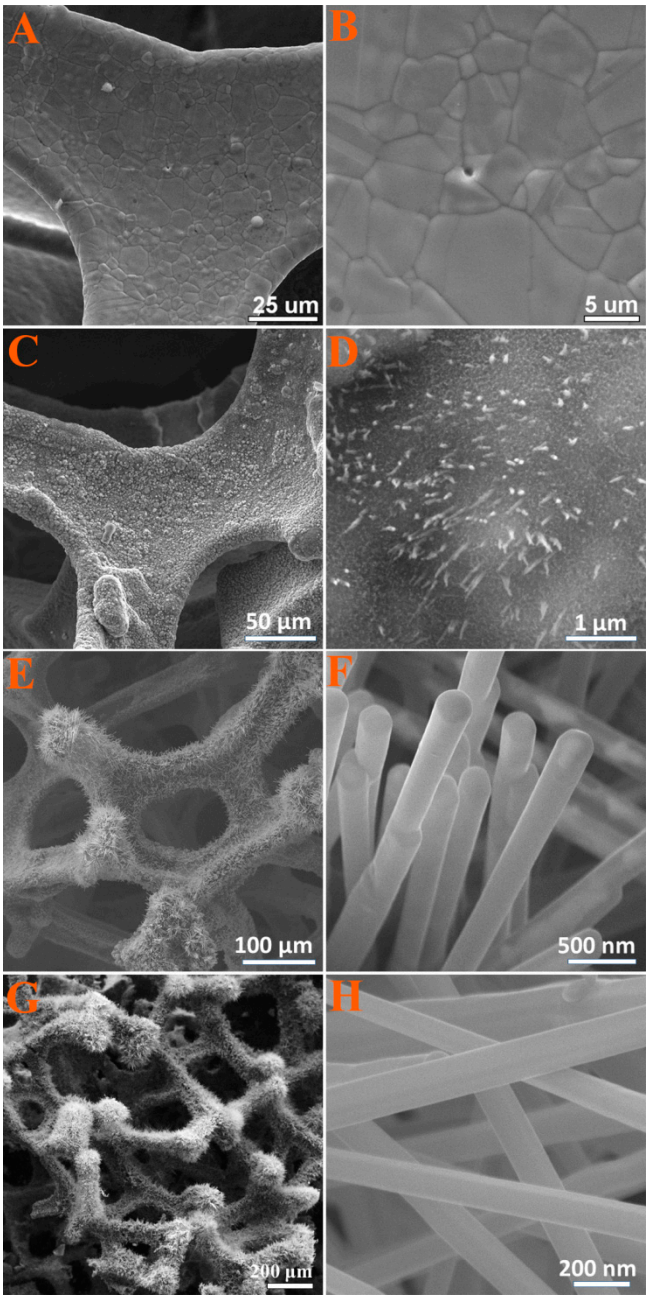

Figure S1. SEM images of Ni_2P@NC nanorod growth from Ni foam after different pyrolysis times: (A, B) 0 min (fresh nickel foam); (C, D) 5 min; (E, F) 30 min and (G, H) 60 min.

Table S1. Commonly reported synthesis methods for nickel phosphides

Nickel phosphide	Morphology	Synthesis	Phosphorus source and precursor
Ni_2P[1]	Hollow spheres	CVD	NaH_2PO_2 + Prepared NiO hollow spheres
Ni_2P[2]	Nanoarray	CVD	NaH_2PO_2 + Prepared $Ni(OH)_2$ nanoarrays
Ni_2P[3]	Nanobelts	CVD	NaH_2PO_2 + $Ni(SO_4)_{0.3}(OH)_{1.4}$ nanobelts
Ni_2P[4]	Nanocrystals	Solution-based method	$C_{24}H_{51}P$ + $C_{10}H_{16}NiO_4$
Ni_2P[5]	Nanoflakes	CVD	NaH_2PO_2 +Prepared $Ni(OH)_2$ nanoflakes
Ni_2P[6, 7]	Nanoparticle	CVD	NaH_2PO_2 + $NiCl_2 \cdot 6H_2O$
Ni_2P[8]	Nanorods	CVD	$NaH_2PO_2 \cdot 6H_2O$ + Prepared $Ni(OH)_2$ nanorods
Ni_2P[9]	Yolk–shell	CVD	PH_3 + Prepared NiO yolk–shell
Ni_3P[10]	Nanoparticles	Solid-State	Phosphorus + Ni
Ni_2P-Ni[11]	Honeycomb	CVD	NaH_2PO_2 + Prepared NiO-Ni honeycombs
Ni_2P-Ni[12]	Nanosheets	Solution-based method	$C_{24}H_{51}PO$ + Prepared $Ni(OH)_2$-Ni nanosheet
Ni_3P-Ni[13]	Arrays	Hydrothermal	$NaH_2PO_2 \cdot H_2O$ + $NiSO_4 \cdot 6H_2O$+Ni foam
Ni_8P_3-Ni[14]	Nanoparticles	CVD	NaH_2PO_2 + Prepared NiO-Ni
NiP_2-Ni[15]	Nanosheets	Solid-State	Red phosphorus+ Ni foam
Ni_2P/C[16]	Carbon support	Solid-State	Red phosphorus+ $Ni(AC)_2 \cdot 6H_2O$ + carbon source
Ni_2P/C[17, 18]	Carbon support	CVD	NaH_2PO_2 + $NiCl_2 \cdot 6H_2O$ + Carbon source
Ni_2P/C[19]	Carbon support	Hydrothermal	Red phosphorus + $NiCl_2 \cdot 6H_2O$ + Carbon nanosheets
Ni_2P/C[20]	Carbon support	Solvothermal	NaH_2PO_2 + $Ni(NO_3)_2$ + glucose
Ni_2P@NC This work	Nanorod arrays		P-containing resin + nickel foam

Key: CVD = Chemical vapor deposition

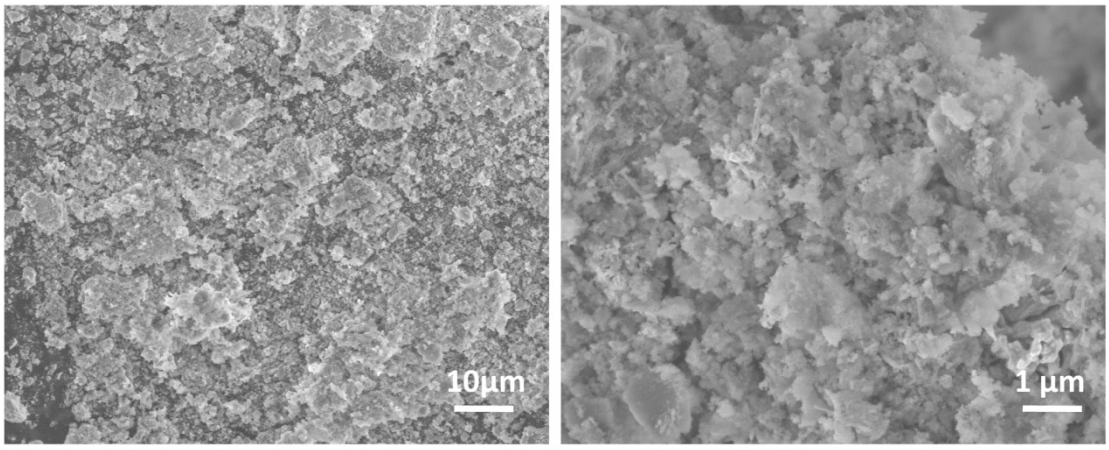

Figure S2. SEM images of Ni_2P.

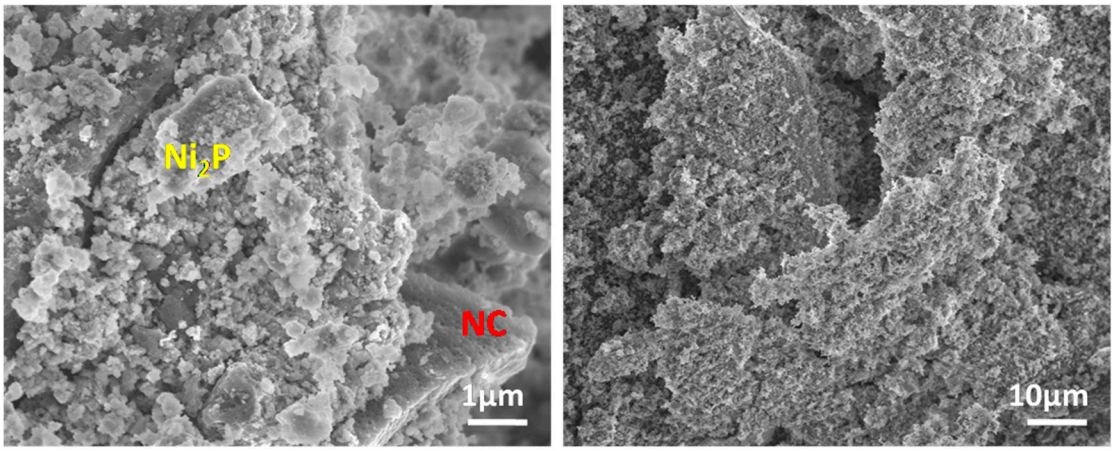

Figure S3. SEM images of Ni_2P/NC.

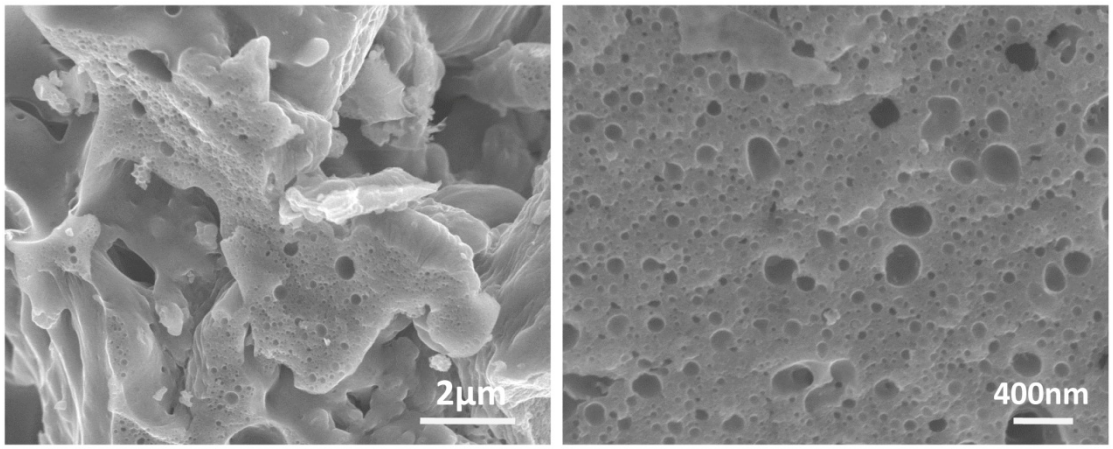

Figure S4. SEM images of NC.

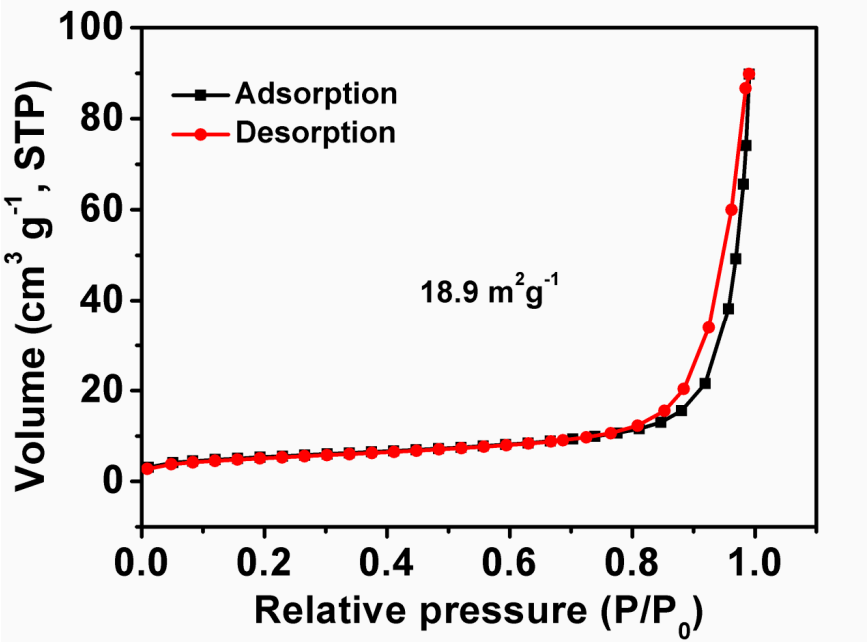

Figure S5. N_2 adsorption–desorption isotherms of Ni_2P.

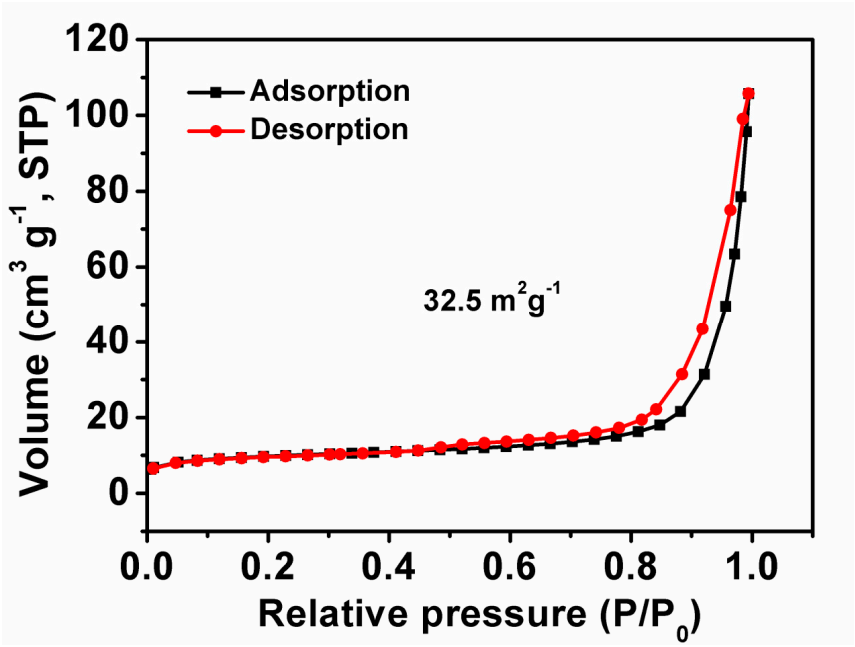

Figure S6. N_2 adsorption–desorption isotherms of Ni_2P/NC.

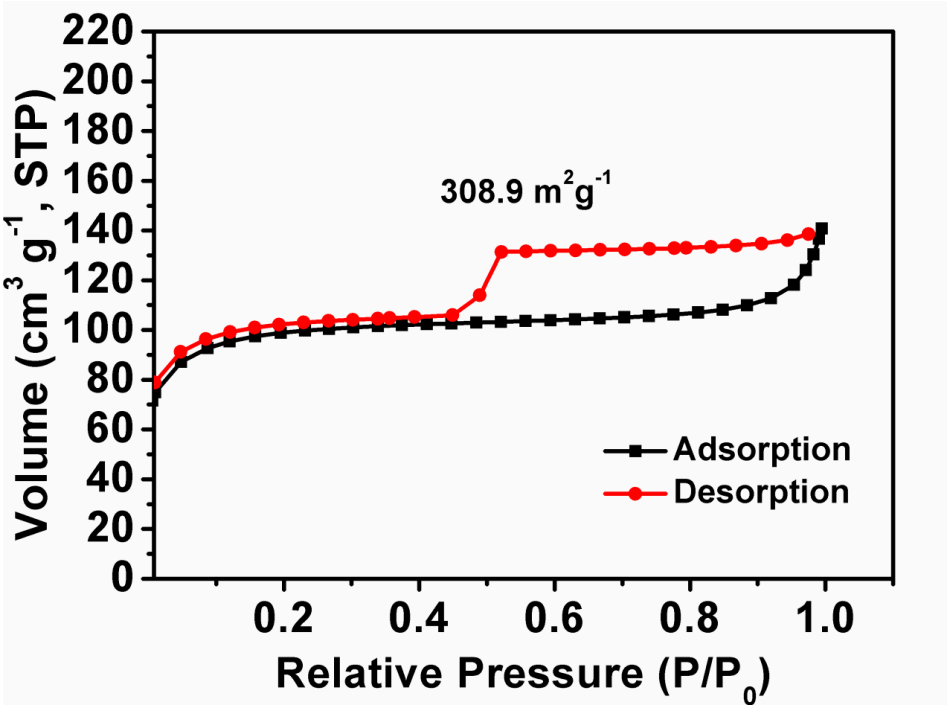

Figure S7. N_2 adsorption–desorption isotherms of NC.

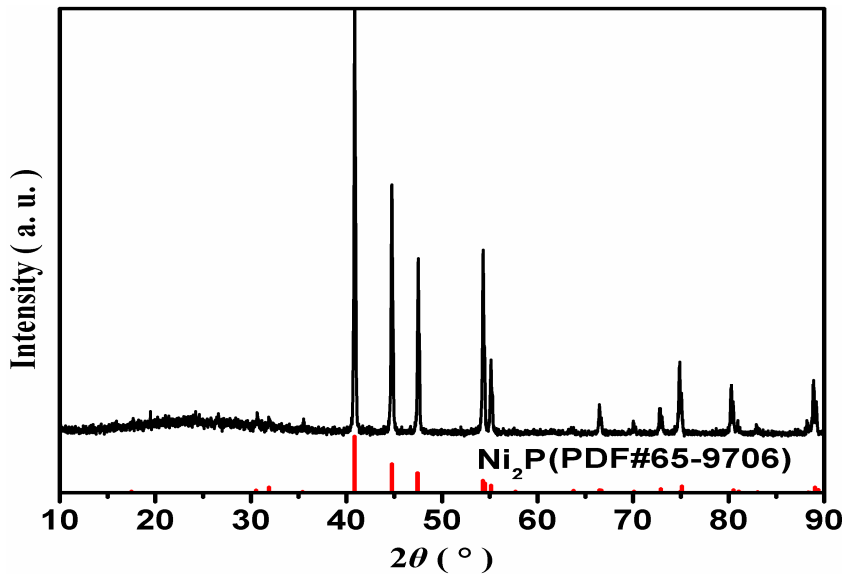

Figure S8. XRD pattern of Ni_2P@NC in 5 min.

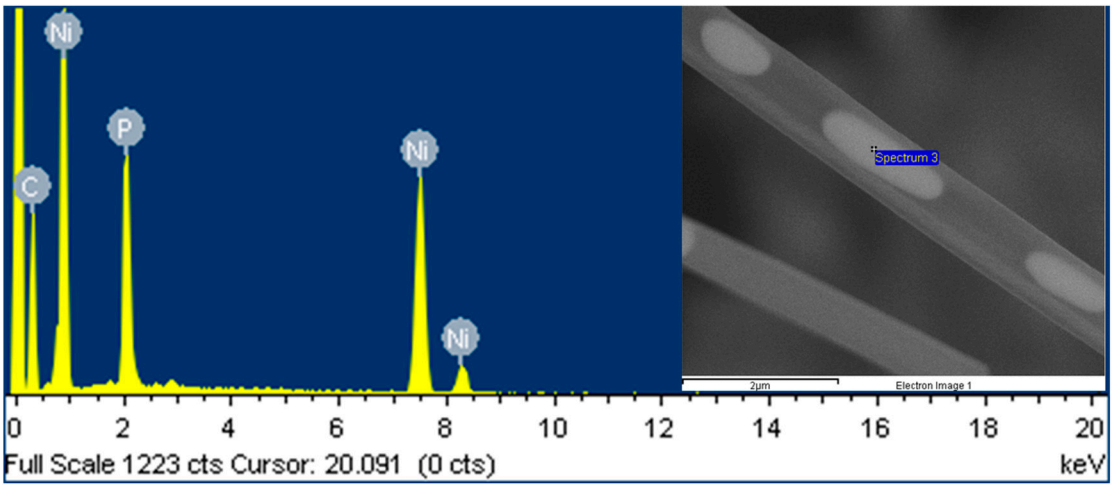

Figure S9. EDS analysis of nanorod array of Ni_2P@NC in 30 min.

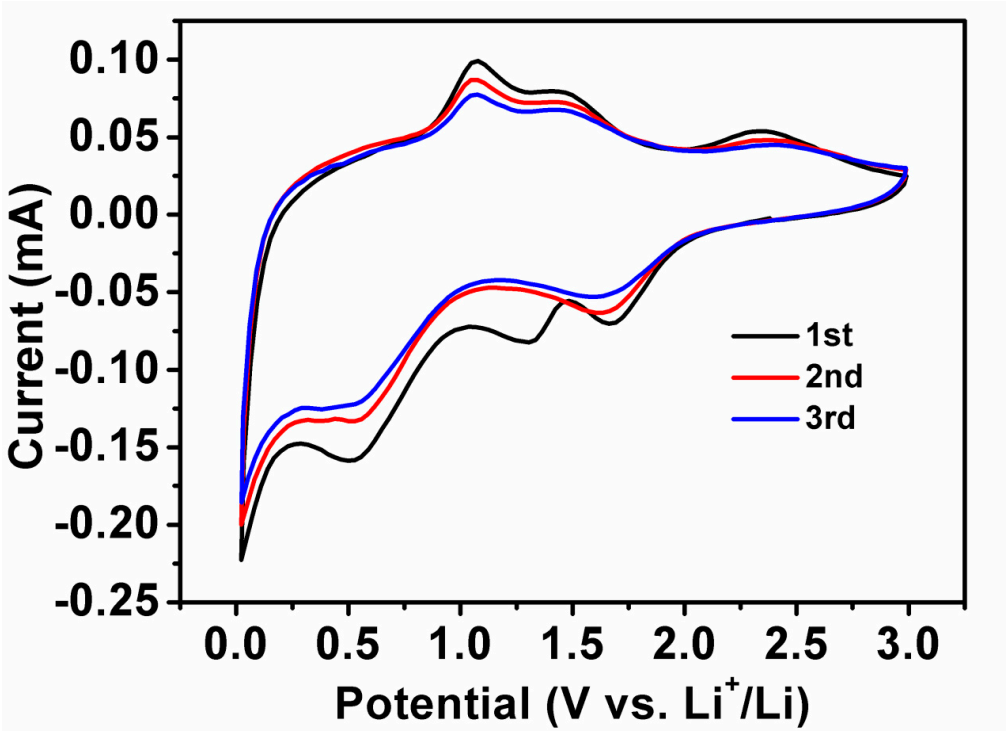

Figure S10. CV curves of Ni_2P powder at 0.2 mV s^{-1} between 0.01 and 3.0 V vs. Li^+/Li.

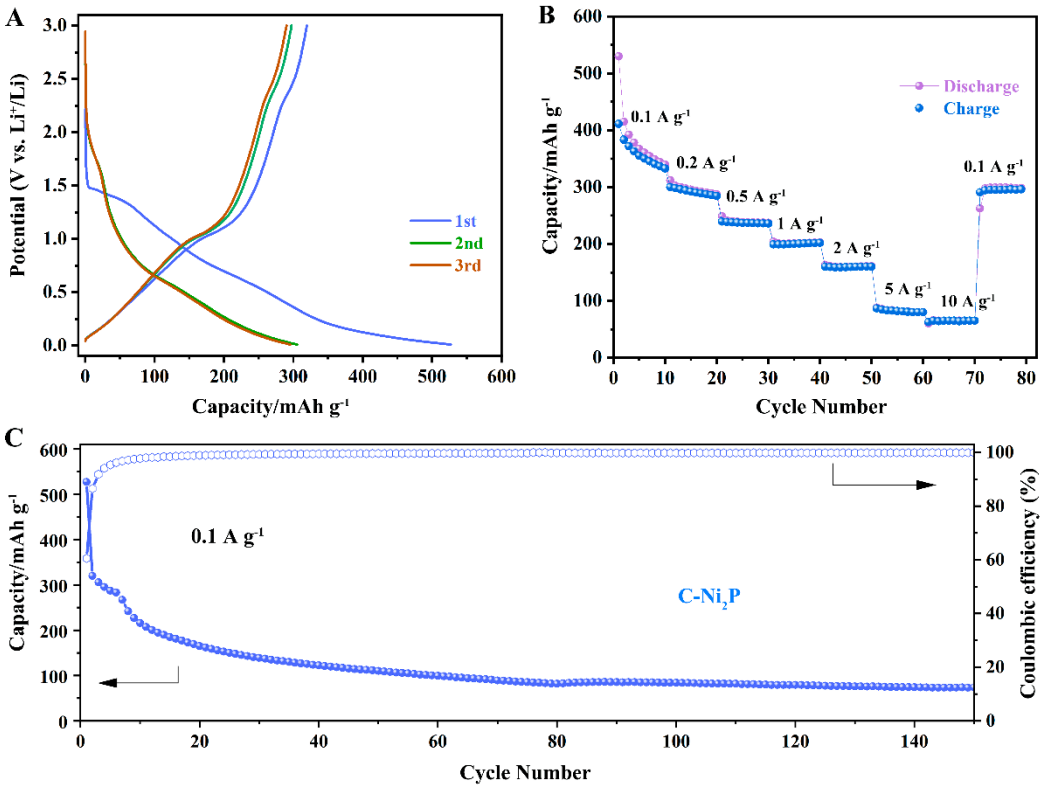

Figure S11. (A) Discharge–charge curves of C-Ni_2P against Li metal in LIB electrolyte at 0.1 A g^{-1}. (B) Rate testing between 0.1 and 10 A g^{-1}. (C) Long-term cycling performance at 0.1 A g^{-1}.

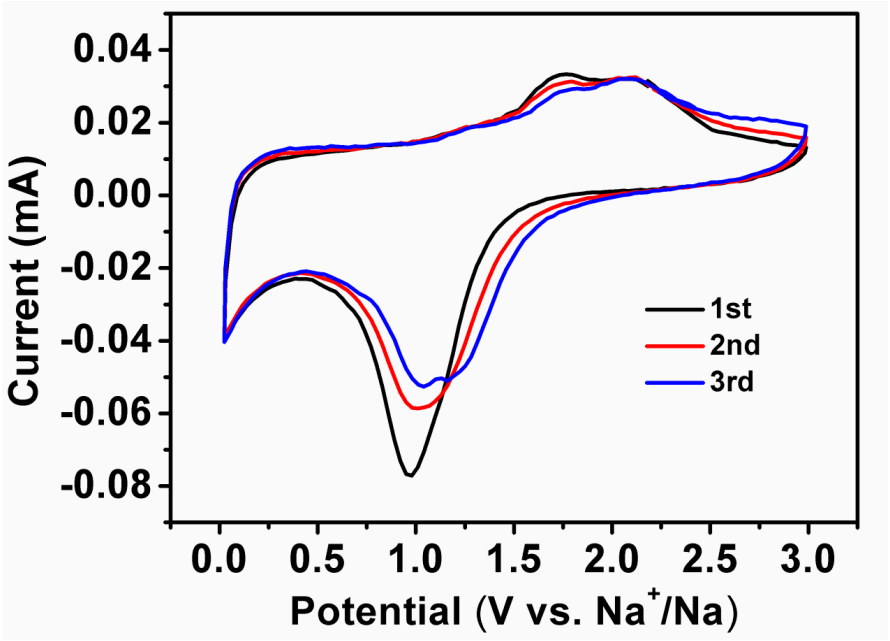

Figure S12. CV curves of Ni_2P powder at 0.2 mV s^{-1} between 0.01 and 3.0 V vs. Na^+/Na.

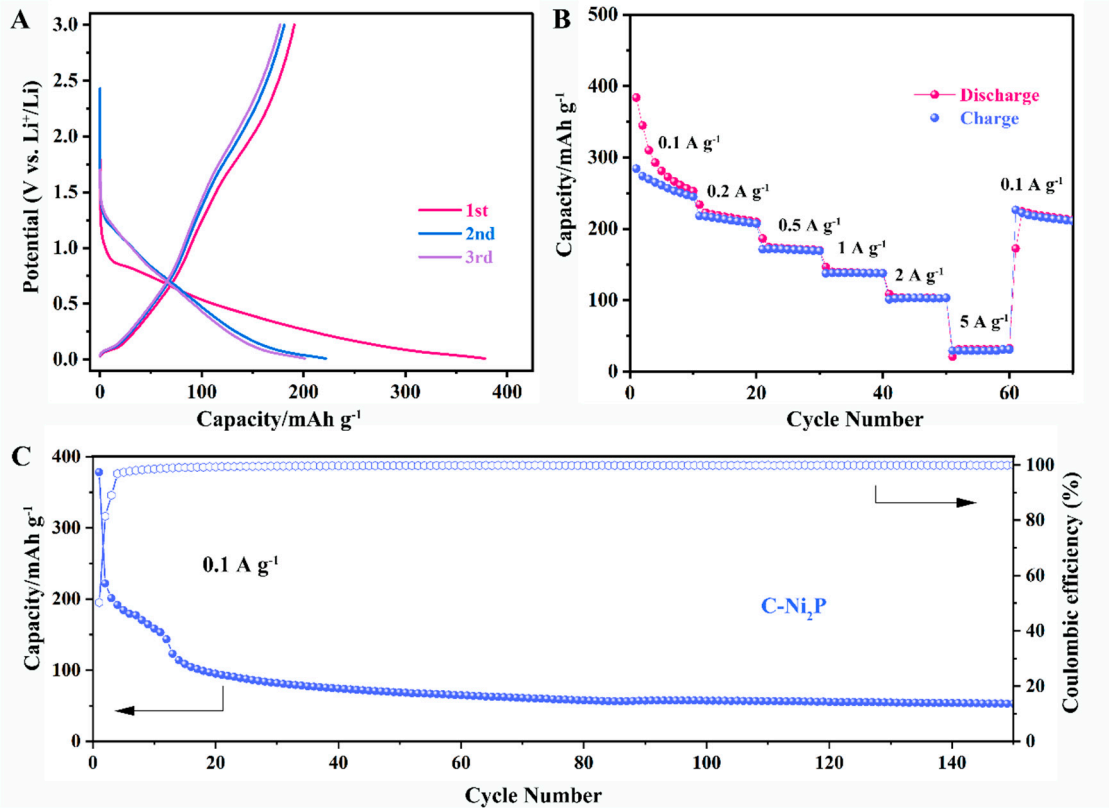

Figure S13. (A) Discharge–charge curves of C-Ni2P against Na metal in SIB electrolyte at 0.1 A g^{-1}. (B) Rate testing between 0.1 and 5 A g^{-1}. (C) Long-term cycling performance at 0.1 A g^{-1}.

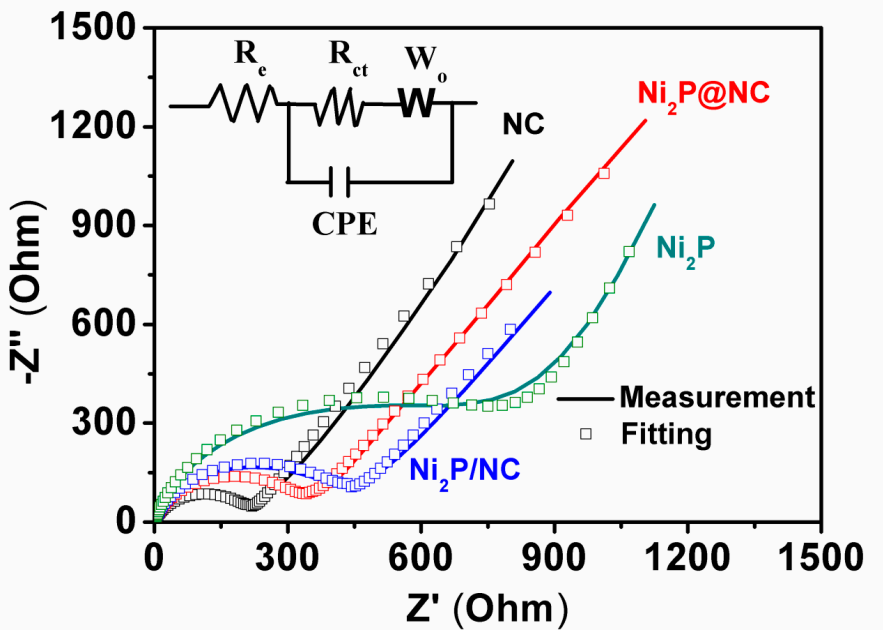

Figure S14. EIS spectra and equivalent circuit for Ni2P@NC, Ni2P/NC, Ni2P and NC as SIB anode materials, where R_e, R_{ct}, CPE and W_o in the fitted equivalent circuit are electrolyte resistance, charge-transfer resistance at the electrode/electrolyte interface,

constant phase element impedance and Warburg impedance, respectively.

Table S2. Cycling performance of reported Ni_2P as LIBs anode material.

Nickel phosphide and Ref.	Maximum current density (mA g^{-1})	Cycles	Discharge capacities (2nd cycle to final cycle mAh g^{-1})	Decay ratio per cycle (%)
Ni_2P@C/CNTs[21]	200	300	453 to 442	0.008
Ni_2P/C[22]	500	400	285 to 265	0.018
Ni_2P@C [23]	200	300	637 to 618	0.009
Ni_2P@C[24]	100	100	756 to 512	0.324
Ni_2P[25]	271	50	573 to 351	0.791
Ni_2P/NG/Ni_2P[26]	300	60	673 to 423	0.619
Ni_2P@C[22]	100	220	487 to 360	0.119
Ni_2P@C[24]	200	100	756 to 512	0.323
Ni_2P@NC (this work)	5000	6000	226 to 170	0.004

Table S3. Cycling performance of reported Ni_2P as SIB anode material.

Nickel phosphide and Ref.	Maximum current density (mA g^{-1})	Cycles	Discharge capacities (2nd cycle to final cycle mAh g^{-1})	Decay ratio per cycle (%)
Ni_2P/NG/Ni_2P [26]	500	300	300 to 188	0.124
Ni_2P@C[24]	100	300	340 to 292	0.047
Ni_2P@PSC[27]	50	100	400 to 295	0.263
Ni_2P@NPC[16]	1000	300	304 to 158	0.161
Ni_2P@C [28]	2000	1500	380 to 104	0.015
Ni2P/3DG [29]	200	100	~880 to 402	0.543
Ni_2P@NC (this work)	2000	2000	179 to 151	0.008

2. Energy calculations for Ni_2P@NC as a LIB and SIB anode material

Determining the possible specific and volumetric energy contributions of the Ni_2P@NC anodes in LIBs and SIBs requires consideration of its voltage range in relation to its capacity range. Over the 0.01 to 3 V cycling range (vs. Li or Na metal), cycling at 0.1 A/g produced impressive specific capacities of 630 and 290 mAh/g, respectively, at the 300^{th} cycle. Fig. S15 shows that the half-cell charge voltage slopes for both LIB and SIB cycling have an initial high capacity/voltage slope (dQ/dV) followed by a lower dQ/dV slope at regions >50% of their full capacity. Since a low average anode voltage is beneficial to the energy density in full cells, it can be advantageous to sacrifice some capacity by choosing a lower voltage cutoff value on the anode. Such a cell would thus require less balancing cathode mass to match the lower capacity. Noting that the average full-cell voltage equals the average anode voltage subtracted from the average cathode voltage, Fig. S15 shows average anode voltages (red plots) preceding all possible cutoff values on the charge plots. Average voltages were calculated by using the sum of all available voltage point values (preceding all possible charge plot voltage points) divided by the number of preceding points. For example, the average voltage preceding the full capacity of 630 mAh/g at the 3 V vs. Li^+/Li cutoff was ~1.5 V, while the average voltage at 400 mAh/g was as low as ~0.55 V.

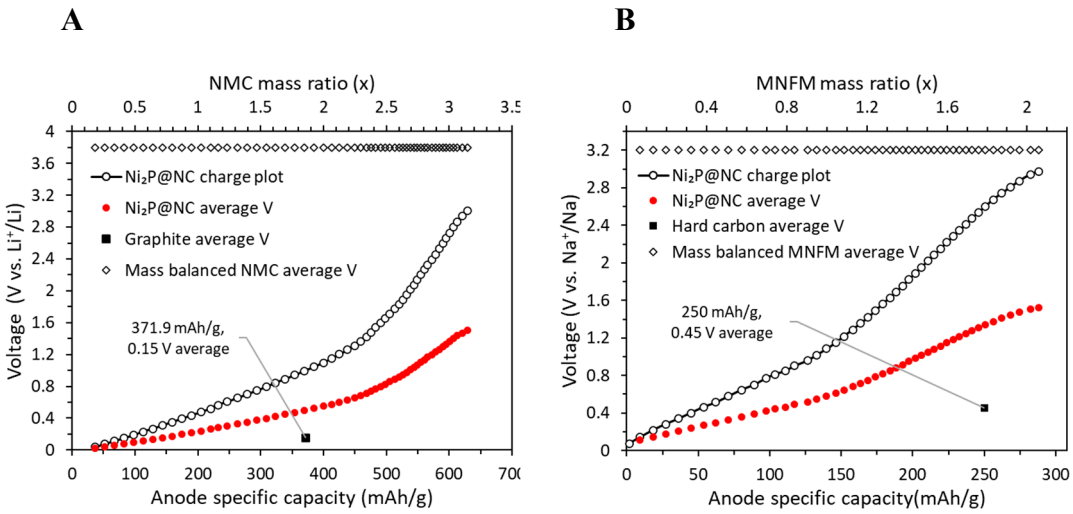

Figure S15. Average voltages of Ni_2P@NC in (A) LIBs and (B) SIBs. (A) Comparison to graphite (0.15 V average) and capacity–mass-balanced $LiNi_{0.3}Mn_{0.3}Co_{0.3}O_2$ (NMC 333: 3.8 V average). (B) Comparison to a typical hard carbon anode (HC: 0.45 V average) and $Na_{0.76}Mn_{0.5}Ni_{0.3}Fe_{0.1}Mg_{0.1}O_2$ (MNFM: 3.2 V average).

Fig. S15 also shows the mass ratio of cathode materials required to balance the capacity of the anode over the full range of possible anode cutoff voltages. The hypothetical cathodes shown are $LiNi_{0.3}Mn_{0.3}Co_{0.3}O_2$ (NMC 333) for LIBs and $Na_{0.76}Mn_{0.5}Ni_{0.3}Fe_{0.1}Mg_{0.1}O_2$ (MNFM) for SIBs, which have maximum specific capacities of ~200 and ~140 mAh/g and average discharge voltages of ~3.8 V vs. Li^+/Li and ~3.2 V vs Na^+/Na, respectively [30,31]. Also shown in Fig. S15 are the standard anodes graphite (371.9 mAh/g at 0.15 V average) and hard carbon (HC: 250 mAh/g at 0.45 V average) for LIBs and SIBs, respectively [32,33]. At this point, the range of cell specific capacities for full cells of Ni_2P@NC/cathode combinations could be calculated along with their average cell voltages.

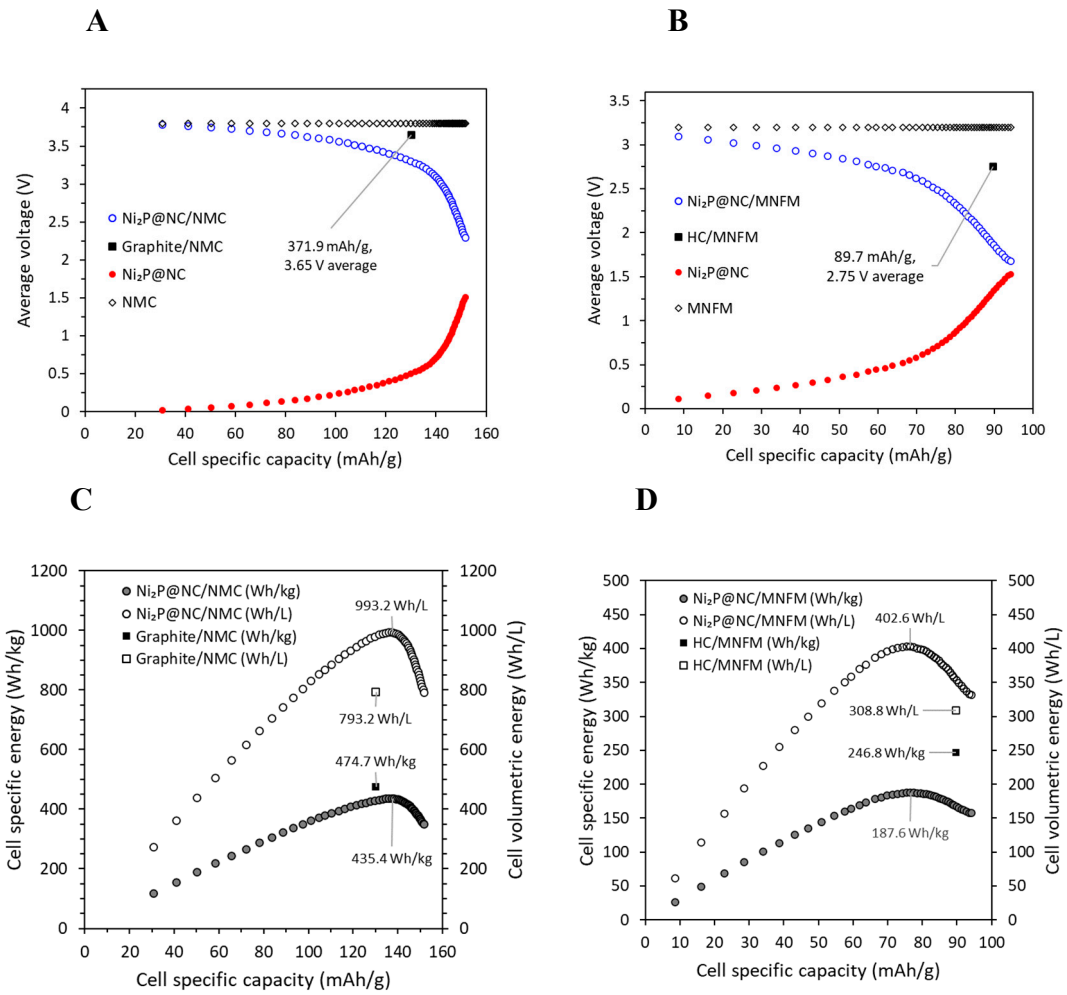

Figure S16. (A and B) Average voltages vs. cell specific capacity of Ni_2P@NC/cathodes in (A) LIBs and (B) SIBs. (C and D) Specific and volumetric energy of Ni_2P@NC/cathodes in (A) LIBs and (B) SIBs with labeled maxima points.

Fig. S16 A and B show the calculated plots of cell specific capacity vs. average cell voltage for the LIB and SIB Ni_2P@NC/cathode pairings over the full range of possible average anode voltage cutoff points. From these plots, the cutoff delivering the maximum specific energy (average cell voltage x cell specific capacity) can be found from the maxima of curve plots (Fig. S16 C and D). In both LIBs and SIBs, no anode voltage cutoff point for a Ni_2P@NC/cathode pairing could produce more specific energy than the standard graphite/NMC or HC/MNFM cells (Fig. S16 C and D). The

maxima were 435.4 Wh/kg for LIBs and 187 Wh/kg for SIBs, compared to 474.7 Wh/kg for graphite/NMC and 246.8 Wh/kg for HC/MNFM. These values amount to an ~8.3 and ~24% decrease, respectively, compared to graphite and HC cells. However, in the case of volumetric energy, there is a calculable improvement over graphite and hard carbon. The calculation of volumetric energy required first calculating the total densities of the active materials used at the mass ratios in cells that yielded the maximum specific energy (Table S4).

Table S4. Density of active materials in cells yielding maximum specific energy.

Ni_2P@NC/NMC LIB	Crystal ρ g/cm^3	Mass g	Volume cm^3	Packing ρ g/cm^3	**Graphite/NMC LIB**	Crystal ρ g/cm^3	Mass g	Volume cm^3	Packing ρ g/cm^3
Ni_2P	7.55 [34]	0.85	0.113	3.775	Graphite	2.26 [37]	1	0.442	1.13
NC*	1.5 [35]	0.15	0.1	0.75	NMC 333	4.5	1.86	0.413	2.25
Ni_2P@NC	4.704	1	0.213	2.352	Cell	3.342	2.86	0.856	1.671
NMC 333	4.5 [36]	2.192	0.487	2.25					
Cell	4.562	3.192	0.7	2.281					
Ni_2P@NC/MNFM SIB	g/cm^3	g	cm^3	g/cm^3	**HC/MNFM SIB**	g/cm^3	g	cm^3	g/cm^3
Ni_2P@NC	4.704	1	0.213	2.352	HC	1.5 [35]	1	0.667	0.75
MNFN	4 [31]	1.205	0.301	2	MNFM	4	1.786	0.446	2
Cell	4.291	2.205	0.514	2.146	Cell	2.503	2.786	1.113	1.251
Note: Packing ρ set to 50% *NC assumed as HC (i.e., low ρ)									

Multiplication of the cell density by the specific energy provided the volumetric energy plots shown in Fig. S16 C and D. Owing to the high density of Ni_2P@NC, the maxima were 993.2 Wh/L for LIBs and 402.6 Wh/L for SIBs, compared to 793.2 Wh/L for graphite/NMC and 308.8 Wh/L for HC/MNFM. These values amount to an impressive ~25.2 and ~30.4% increase, respectively, compared to graphite and HC cells.

Therefore, while these values were theoretically determined, the use of the above method gives a strong indication of the material's possible volumetric energy contribution. Furthermore, the above results reveal the impact of choosing the optimal voltage cutoff for the anode in relation to cathode balancing for finding the energy maxima. Finally, Fig. S17 completes the plots in Fig. S15 to show the positions of voltage cutoffs and cathode mass balance values for maximum energy usage (data values shown in Table S5).

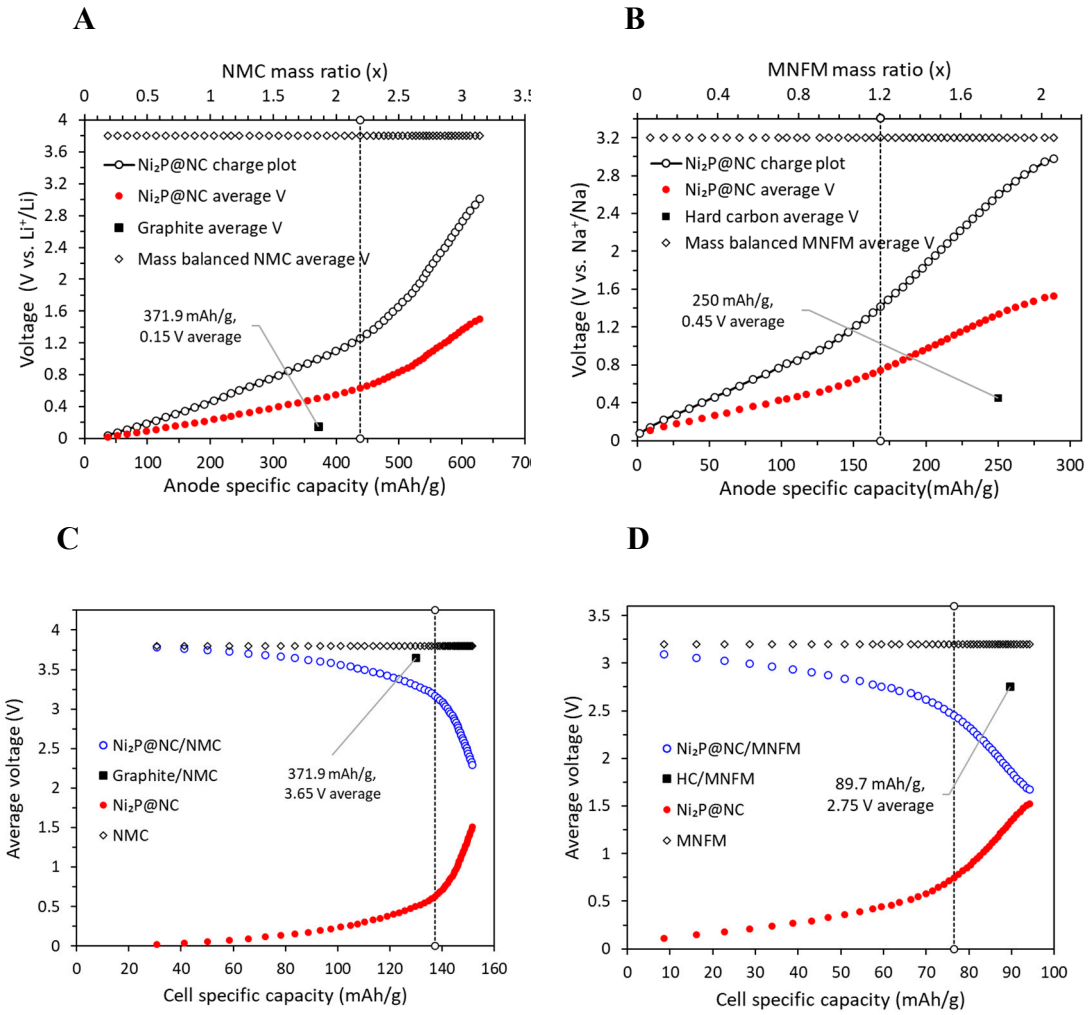

Figure S17. Maximum energy density cutoff capacities and related voltages for Ni_2P@NC in LIBs and SIBs demarked by dashed lines (see Table S4 for cutoff values).

Table S5. Parameters for maximized energy of active materials.

1. LIBS												
Ni_2P @ NC (anode)				**NMC 333 (cathode)**			**Ni_2P @ NC/NMC 333 (cell)**					
mAh/g	V cutoff	Ave. V	g	mAh/g	Ave. V	g	mAh/g	Ave. V	V cutoff	Wh/kg	g/cm3	Wh/L
438.4	1.26	0.63	1	200	3.8	2.19	137.3	3.17	2.54	435.4	2.28	993.2
2. SIBS												
Ni_2P @ NC (anode)				**MNFM (cathode)**			**Ni_2P @ NC/MNFM (cell)**					
mAh/g	V cutoff	Ave. V	g	mAh/g	Ave. V	g	mAh/g	Ave. V	V cutoff	Wh/kg	g/cm3	Wh/L
168.6	1.42	0.75	1	140	3.2	1.2	76.5	2.45	1.78	187.63	2.15	402.59

References

1. Sun, H.; Xu, X.; Yan, Z.; Chen, X.; Cheng, F.; Weiss, P. S.; Chen, J., Porous Multishelled Ni_2P Hollow Microspheres as an Active Electrocatalyst for Hydrogen and Oxygen Evolution. *Chem. Mater.* **2017,** *29*, 8539-8547.
2. Chen, T.; Liu, D.; Lu, W.; Wang, K.; Du, G.; asiri, A. M.; Sun, X., Three-Dimensional Ni_2P Nanoarray: an Efficient Catalyst Electrode for Sensitive and Selective Nonenzymatic Glucose Sensing with High Specificity. *Anal. Chem.* **2016,** *88*, 7885-7889.
3. Jin, Y.; Zhao, C.; Wang, L.; Jiang, Q.; Ji, C.; He, X., Preparation of Mesoporous Ni_2P Nanobelts with High Performance for Electrocatalytic Hydrogen Evolution and Supercapacitor. *Int. J. Hydrogen Energy* **2018,** *43*, 3697-3704.
4. Chen, Y.; Qin, Z., General Applicability of Nanocrystalline Ni_2P as a Noble-Metal-Free Cocatalyst to Boost Photocatalytic Hydrogen Generation. *Catal. Sci. Technol.* **2016,** *6*, 8212-8221.
5. Mai, Y.-J.; Xia, X.; Jie, X.-H., Cross-Linked Hierarchical Arrays of Ni_2P Nanoflakes Prepared Via Directional Phosphorization and Their Applications for Advanced Alkaline Batteries. *J. Power Sources* **2017,** *367*, 116-121.
6. Liu, G.; He, D.; Yao, R.; Zhao, Y.; Li, J., Enhancing the Water Oxidation Activity of Ni_2P Nanocatalysts By Iron-Doping and Electrochemical Activation. *Electrochimi. Acta* **2017,** *253*, 498-505.
7. Stern, L.-A.; Feng, L.; Song, F.; Hu, X., Ni_2P as A Janus Catalyst for Water Splitting: the Oxygen Evolution Activity of Ni_2P Nanoparticles. *Energy Environ. Sci.* **2015,** *8*, 2347-2351.
8. Li, Q.; Ma, J.; Wang, H.; Yang, X.; Yuan, R.; Chai, Y., interconnected Ni_2P Nanorods Grown on Nickel Foam for Binder Free Lithium Ion Batteries. *Electrochim. Acta* **2016,** *213*, 201-206.
9. Cheng, J.; Zhao, D.; Fan, L.; Wu, X.; Wang, M.; Zhang, N.; Sun, K., Ultra-High Rate Li-S Batteries Based on A Novel Conductive Ni_2P Yolk-Shell Material as the Host for the S Cathode. *J. Mater. Chem. A* **2017,** *5*, 14519-14524.

10. Laursen, A. B.; Wexler, R. B.; Whitaker, M. J.; Izett, E. J.; Calvinho, K. U. D.; Hwang, S.; Rucker, R.; Wang, H.; Ji, J.; Garfunkel, E.; Greenblatt, M.; Rappe, A. M.; Dismukes, G. C., Climbing the Volcano of Electrocatalytic Activity while Avoiding Catalyst Corrosion: Ni_3P, a Hydrogen Evolution Electrocatalyst Stable in Both Acid and Alkali. *Acs Catal.* **2018,** *8*, 4408-4419.

11. Wang, X. D.; Cao, Y.; Teng, Y.; Chen, H. Y.; Xu, Y. F.; Kuang, D. B., Large-Area Synthesis of A Ni_2P Honeycomb Electrode for Highly Efficient Water Splitting. *ACS Appl. Mater. interfaces* **2017,** *9*, 32812-32819.

12. Shi, Y.; Xu, Y.; Zhuo, S.; Zhang, J.; Zhang, B., Ni_2P Nanosheets/Ni Foam Composite Electrode for Long-Lived and Ph-Tolerable Electrochemical Hydrogen Generation. *ACS Appl. Mater. interfaces* **2015,** *7*, 2376-2384.

13. Liu, S.; Feng, J.; Bian, X.; Liu, J.; Xu, H., Electroless Deposition of Ni_3P-Ni Arrays on 3-D Nickel Foam as A High Performance Anode for Lithium-Ion Batteries. *RSC Adv.* **2015,** *5*, 60870-60875.

14. Chen, G.-F.; Ma, T. Y.; Liu, Z.-Q.; Li, N.; Su, Y.-Z.; Davey, K.; Qiao, S.-Z., Efficient and Stable Bifunctional Electrocatalysts Ni/Ni_xm_y (M = P, S) for Overall Water Splitting. *Adv. Funct. Mater.* **2016,** *26*, 3314-3323.

15. Wang, X.; Li, W.; Xiong, D.; Liu, L., Fast Fabrication of Self-Supported Porous Nickel Phosphide Foam for Efficient, Durable Oxygen Evolution and Overall Water Splitting. *J. Mater. Chem. A* **2016,** *4*, 5639-5646.

16. Shi, S.; Li, Z.; Sun, Y.; Wang, B.; Liu, Q.; Hou, Y.; Huang, S.; Huang, J.; Zhao, Y., A Covalent Heterostructure of Monodisperse Ni_2P Immobilized on N, P-Co-Doped Carbon Nanosheets for High Performance Sodium/Lithium Storage. *Nano Energy* **2018,** *48*, 510-517.

17. Sun, Y.; Zhang, T.; Li, X.; Bai, Y.; Lyu, X.; Liu, G.; Cai, W.; Li, Y., Bifunctional Hybrid Ni/Ni_2P Nanoparticles Encapsulated By Graphitic Carbon Supported with N, S Modified 3D Carbon Framework for Highly Efficient Overall Water Splitting. *Adv. Mater. interfaces* **2018,** *5*, 1800473.

18. Sun, T.; Dong, J.; Huang, Y.; Ran, W.; Chen, J.; Xu, L., Highly Active and Stable Electrocatalyst of Ni_2P Nanoparticles Supported on 3D Ordered Macro-/Mesoporous Co-N-Doped Carbon for Acidic Hydrogen Evolution Reaction. *J. Mater. Chem. A* **2018,** *6*, 12751-12758.

19. Li, Y.; Cai, P.; Ci, S.; Wen, Z., Strongly Coupled 3D Nanohybrids with Ni_2P/Carbon Nanosheets as Ph-Universal Hydrogen Evolution Reaction Electrocatalysts. *Chemelectrochem* **2017,** *4*, 340-344.

20. Feng, Y.; Zhang, H.; Mu, Y.; Li, W.; Sun, J.; Wu, K.; Wang, Y., Monodisperse Sandwich-Like Coupled Quasi-Graphene Sheets Encapsulating Ni_2P Nanoparticles for Enhanced Lithium-Ion Batteries. *Chemistry* **2015,** *21*, 9229-9235.

21. Yao, C.; Xu, J.; Shen, Y.; Xie, A., Synthesis and Excellent Performance of Porous Ni_2P@C/Cnts Nanocomposite Derived From Ni-Mofs as an Anode for Lithium-Ion Batteries. *int. J. Energy Res.* **2022,** *46*, 10875-10884.

22. Zhang, R. Z.; Zhu, K. J.; Huang, J. D.; Yang, L. Y.; Li, S. T.; Wang, Z. Y.; Xie, J. R.; Wang, H.; Liu, J., Ultrafine Ni_2P Nanoparticles Embedded in one-Dimensional Carbon Skeleton Derived From Metal-Organic Frameworks Template as a High-Performance Anode for Lithium Ion Battery. *J. Alloys Compd.* **2019,** *775*, 490-497.

23. Bai, Y.; Zhang, H.; Fang, L.; Liu, L.; Qiu, H.; Wang, Y., Novel Peapod Array of Ni_2P@Graphitized Carbon Fiber Composites Growing on Ti Substrate: A Superior Material for Li-Ion Batteries and the Hydrogen Evolution Reaction. *J. Mater. Chem. A* **2015,** *3*, 5434-5441.

24. Zheng, J.; Huang, X.; Pan, X.; Teng, C.; Wang, N., Yolk-Shelled Ni_2P@Carbon Nanocomposite as High-Performance Anode Material for Lithium and Sodium Ion Batteries. *Appl. Surf. Sci* **2019,** *473*, 699-705.

25. Kim, C.; Kim, H.; Choi, Y.; Lee, H. A.; Jung, Y. S.; Park, J., Facile Method To Prepare for the Ni_2P Nanostructures with Controlled Crystallinity and Morphology as Anode Materials of Lithium-Ion Batteries. *ACS Omega* **2018,** *3*, 7655-7662.

26. Dong, C.; Guo, L.; He, Y.; Chen, C.; Qian, Y.; Chen, Y.; Xu, L., Sandwich-Like Ni_2P Nanoarray/Nitrogen-Doped Graphene Nanoarchitecture as A High-Performance Anode for Sodium and Lithium Ion Batteries. *Energy Storage Mater.* **2018,** *15*, 234-241.

27. Zhou, D.; Xue, L.-P.; Wang, N., Robustly Immobilized Ni_2P Nanoparticles in Porous Carbon Networks Promotes High-Performance Sodium-Ion Storage. *J. Alloys Compd.* **2019,** *776*, 912-918.

28. Liang, J.; Zhu, G.; Zhang, Y.; Liang, H.; Huang, W., Conversion of Hydroxide into Carbon-Coated Phosphide Using Plasma for Sodium Ion Batteries. *Nano Res.* **2022,** *15*, 2023-2029.

29. Li, H.; Wang, X.; Zhao, Z.; Tian, Z.; Zhang, D.; Wu, Y., Ni_2P Nanoflake Array/Three Dimensional Graphene Architecture as Integrated Free-Standing Anode for Boosting the Sodiation Capability and Stability. *ChemElectroChem* **2019,** *6*, 404-412.

30. Shaju, K.M., Subba Rao, G.V., Chowdari, B.V.R. (2002-11-21). Performance of layered $Li(Ni_{1/3}Co_{1/3}Mn_{1/3})\ O_2$ as cathode for Li-ion batteries. *Electrochimica Acta*. **2002**, *48 (2)* : 145-151.

31. Keller, M.; Buchholz, D.; Passerini, S., Layered Na-Ion Cathodes with Outstanding Performance Resulting from the Synergetic Effect of Mixed P- and O-Type Phases. *Adv. Energy Mater.* **2016**, *6*, 1501555.

32. Mao, C.; Wood, M.; David, L.; Jin An, S.; Yangping Sheng, Y.; Du, Z.; Meyer, H.; Rose, E.; Ruther R. E.; Wood, D. L. Selecting the Best Graphite for Long-Life, High-Energy Li-Ion Batteries. *J. Electrochem. Soc.* **2018**, *165*, A1837.

33. Moon, H.; Innocenti, A.; Liu, H.; Zhang, H.; Weil, M.; Zarrabeitia, Passerini, S. Hard carbon cycling Bio-Waste-Derived Hard Carbon Anodes Through a Sustainable and Cost-Effective Synthesis Process for Sodium-Ion Batteries. *ChemSusChem*. **2023**, *16*, e202201713.

34. Jain, A.; Ong, S. P.; Hautier, G.; Wei Chen, W.; Richards, W. D.; Dacek, S.; Cholia, S.; Gunter, D.; Skinner, D.; Ceder, G.; and Kristin A. Persson, K. A., Commentary: The Materials Project: A materials genome approach to accelerating materials innovation. *APL Materials* 1, 011002 (**2013**).

35. Pistoia, G., Lithium-ion Batteries; Advances and Applications. *Elsevier Ltd.* **2014**, 2, 3, 25.

36. Yin, S.; Rho, Y.; Swainson I.; Nazar L., X-ray/Neutron Diffraction and Electrochemical Studiesof Lithium De/Re-Intercalation in $Li_{1-x}Co_{1/3}Ni_{1/3}Mn_{1/3}O_2$ (x = 0⟶1). *Chemistry of materials*. **2006**, 18, *7*, 1901-1910.

37. Burchell, T. D.; McEnaney, B., Carbon Materials for Advanced Technologies (Structure and Bonding in Carbon Materials). *Elsevier Ltd*. **1999,** 1, 2.2, 5.